



Petrophysical Correlations for the Permeability of Coquinas (Carbonate Rocks)

M. C. O. Lima¹ · E. M. Pontedeiro^{1,3} · M. Ramirez² · A. Boyd¹ · M. Th. van Genuchten^{3,5} · L. Borghi⁴ · P. Couto¹ · A. Raouf³ 

Received: 10 March 2020 / Accepted: 2 September 2020 / Published online: 4 October 2020
© The Author(s) 2020

Abstract

The pore structure of many carbonate formations is known to be very complex and heterogeneous. Heterogeneity is manifested by the presence of different types, sizes, and shapes of pores resulting from sedimentation and diagenetic actions. These complexities greatly increase uncertainties in estimated rock hydraulic properties in that different permeability values may occur for samples having similar porosities. In order to understand the effects of pore structure and heterogeneity, petrophysical analyses were performed on coquina samples from the Morro do Chaves Formation (Barremian, Sergipe-Alagoas Basin), which is an analogue of Brazilian Pre-salt oil reservoirs of Itapema Formation in the Santos Basin. Routine core analyses, and NMR and MICP measurements were carried out to obtain pore body and pore throat distributions. Obtained T_2 relaxation times were converted to pore size radii by matching the NMR and MICP curves. Pore-scale imaging and pore network modelling were performed using microCT scans and the PoreFlow software, respectively. Calculated permeabilities using PoreFlow showed excellent agreement with the routine laboratory measurements. Samples having pore bodies with a higher coordination number showed much larger permeabilities at similar porosities. This study includes a statistical analysis of various features that caused the observed differences in permeability of the coquinas, including the role of connectivity of the entire porous system. Limitations and challenges of the various techniques, and the imaging and pore-scale flow simulations, are discussed.

Keywords Carbonate rocks · Nuclear magnetic resonance · Image processing · PoreFlow · Permeability

✉ A. Raouf
a.raouf@uu.nl

¹ Department of Civil Engineering, COPPE, Federal University of Rio de Janeiro, Rio de Janeiro, Brazil

² Department of Mechanical Engineering, COPPE, Federal University of Rio de Janeiro, Rio de Janeiro, Brazil

³ Department of Earth Sciences, Utrecht University, Utrecht, The Netherlands

⁴ Department of Geology, LAGESED, Federal University of Rio de Janeiro, Rio de Janeiro, Brazil

⁵ Center for Environmental Studies, CEA, São Paulo State University, Rio Claro, São Paulo, Brazil

1 Introduction

Carbonate rocks contain approximately 50% of the world's hydrocarbon reserves (Teles et al. 2016). Because of their wide distribution and importance, carbonate rocks are now increasingly being studied at a range of scales and from various perspectives, especially since the discovery of Brazilian Pre-salt reservoirs in the Santos Basin, an Eastern Brazilian Continental Margin basin. Petrophysical analyses of these rocks indicate extreme heterogeneity in their lithology. Sedimentation and diagenetic action much affected their pore and particle size distributions and original shape (Sun et al. 2016), ultimately reflected in the permeability and percolation properties of these rocks (Lima et al. 2019). Understanding the petrophysical properties of carbonate rocks is essential for better assessment and exploration of hydrocarbon reservoirs (Sun et al. 2016). Like other physical properties of porous materials, permeability is a function of the complex microstructure of the rock involved (Mostaghimi et al. 2013). Although permeability is often assumed to be a relatively simple function of porosity (Kaufmann 2009), in reality this property is also a function of grain size, pore geometry, and the pore size distribution, including pore connectivity and tortuosity (Zhou et al. 2019).

Nuclear magnetic resonance (NMR) and other imaging techniques are very much facilitating rapid and non-destructive petrophysical characterizations of carbonate rocks and other porous media (Cnudde and Boone 2013; Fleury and Romero-Sarmiento 2016; Li et al. 2017). With NMR, the pore space interpretation is evaluated indirectly through the excitation of the nuclear spins, mainly ^1H contained in the saturating fluid molecules. In addition to porosity, the technique is able to provide a pseudo-pore size distribution and, consequently, provides an attractive means for estimating the permeability (Chi and Heidari 2016). Typically, the pore size distribution of a rock sample drives the distribution of transverse relaxation times (referred to as T_2), determined by mathematical inversion of relaxation measurements (Buttler et al. 1981). At the limit of the fast diffusion regime, the relaxation time, T_2 , of a fluid saturating a porous medium is given by

$$\left(\frac{V}{S}\right)_{\text{pore}} = \rho_2 T_2 \quad (1)$$

where ρ_2 represents the surface relaxativity. This equation shows that relaxation times of fluids inside pores are inversely proportional to the pore surface to volume ratio, defined as S/V in Eq. (1), with the scaling of this relationship being the surface relaxativity, ρ_2 . Relaxation at pore surfaces is known to be much faster than that of the bulk fluid phase because of interactions between the solid and fluid molecules in the immediate vicinity of surfaces (Chang et al. 2004). Since ρ_2 represents the strength of the relaxation at pore surfaces, it depends on properties specific to the solid surface and the fluid involved, from which a relationship between relaxation time and pore size can be established (e.g. Wong 1999). The surface relaxativity represents the decay speed of a polarized spin when it interacts with the pore wall. This parameter hence depends on the pore surface, mineralogy, and presence of clay, as well as the saturating fluid involved, thus imposing great uncertainties in terms of its measurement (Souza et al. 2013).

The pore system of a rock can be represented by a pore network consisting of pore bodies (corresponding to the largest voids) and pore throats (connections between the pore bodies) that are responsible for flow (Dong and Blunt 2009; Raouf et al. 2013; among others). A useful analysis complementary to NMR is the characterization of the distribution of pore apertures (e.g. their radii) using mercury intrusion capillary

pressure (MICP). MICP techniques were designed initially to estimate the permeability of relatively small and irregular samples (Purcell 1949), as opposed to measurements by gas injection, which require more regular formats to be accurate. MICP measurements are usually taken by injecting the non-wetting fluid under pressure, with a series of pressure increments until the sample is completely filled. Pore bodies with their larger throats are invaded then typically first at the lower pressures, followed by connecting smaller pore throats at the higher pressures (Brown 2015). By hypothesizing the pore system as a bundle of capillary tubes with different diameters, each capillary pressure increment, P_c , can be related to the pore throat radius, R_t , through the Washburn equation (Washburn 1921):

$$P_c = -\frac{2\sigma \cos \theta}{R_t} \quad (2)$$

where σ is the interfacial tension of mercury with air (dynes/cm² or mN/m²) and θ is the contact angle of mercury with air (°).

An important application of NMR and MICP techniques is the integration of their results to determine the surface relaxativity, a parameter that is essential for calibration of the relaxation time curves T_2 to obtain the pore size distribution (Wong 1999; Fleury and Romero-Sarmiento 2016). Approximating the pore network as a bundle of cylindrical capillary tubes of radius r , the pore structure can be correlated with T_2 by means of the surface relaxativity ρ_2 according to:

$$\left(\frac{S}{V}\right)_{\text{cylinder}} = \frac{2\pi r l}{\pi r^2 l} = \frac{2}{r} \rightarrow r_{\text{cylinder}} = 2\rho_2 T_2 \quad (3)$$

where l is the length of the capillary. The value 2 in the above equation is a pore shape parameter needed to convert the ratio (S/V) in Eq. (1) to pore throat radii, which can be changed to 3 for spherical pores. Thus, once a correlation between the NMR and MICP curves is obtained, ρ_2 can be adjusted until the two curves are consistent (Souza et al. 2013). Combining the NMR and MICP measurements will not yield good results if no correlation exists between the pore size distribution curves and the corresponding pore throats (Mesquita et al. 2016).

Basic and special petrophysical studies are crucial for accurate reservoir descriptions and related computer simulations. These techniques allow measurements of very small (nano- to micron-scale) pores, leading to results that are independent of their shape (Oliveira et al. 2019). To obtain a better understanding, in addition to calculating porosity, pore connections need to be observed. Beginning in the 1990s, 3D image analysis has been used extensively in the petroleum industry to more quickly and reliably obtain rock sample information (Dernaika et al. 2018; Jin et al. 2018). X-ray microtomography images make it now possible to visualize in more detail the internal part of a sample, thus corroborating qualitative and quantitative evaluations of the physical properties and the flow dynamics of a sample (Cnudde and Boone 2013; Ravlo et al. 2016). This approach addresses deficiencies that larger-scale laboratory measurements often have. However, the extraction of information from 3D images still involves inherent ambiguities such as properly distinguishing between pore bodies and pore throats. To address some of these issues, algorithms have been developed to improve the extraction of the networks, sometimes referred to as “networking” or “skeletonization” (e.g. Dong and Blunt 2009). The combined use of laboratory experiments and 3D image analyses should ensure a better understanding of the structure of the rock pore network.

Another integration of 3D imaging techniques and NMR results to estimate the permeability of carbonate rock samples was suggested by Chi and Heidari (2016). They developed a new approach to estimate directional permeability by incorporating a connectivity factor into a conventional NMR-based permeability model. The anisotropic permeability used for calibration and subsequent tests were obtained using lattice Boltzmann modeling (LBM) of microtomographic images. Still, as pointed out by Mostaghimi et al. (2013) and others, LBM methods are computationally very demanding, which restricts their use in some cases.

Recently, pore network models (PNMs) have become popular to improve the description of multi-phase systems. Their use has improved our understanding of macro-scale (or continuum-scale) fluid flow and contaminant transport processes by highlighting the basic pore-scale basis of the various processes involved (Raouf et al. 2013; de Vries et al. 2017). Pore-scale models are not necessarily a substitute for experimental methods, but rather serve as a complement to better understand the experimental data and their uncertainties, and allowing one to replicate experimental conditions (Raouf et al. 2012; Gundogar et al. 2016).

This study focuses on the effects of pore structure, pore size distribution, and connectivity on the relationship between porosity and the permeability. For this purpose, we characterized porosity and permeability data of samples using basic petrophysics. NMR and MICP experiments were performed to obtain the pore and throat size distribution curves, which helped to obtain a better description of the pore systems involved. Microtomographic images were analysed in attempts to better understand and describe the connectivity of the entire system.

2 Geological Context

Our studies were carried out using carbonate rock samples (coquinas) from the Sergipe-Alagoas Basin, located in Northeastern Brazil, which at present constitutes a passive margin basin evolved from rifting processes that caused the opening of the South Atlantic Ocean in the Cretaceous. These processes have been widely studied since they provide the most complete sedimentary succession of the Eastern Continental Margin of Brazil (Feijó and Vieira 1991; Souza et al. 2013). The Morro do Chaves Formation, belonging to this basin, is defined as a coquina (carbonate) succession of the local Jiquiá stage (late Barremian to early Aptian) interbedded with siliciclastic rocks, varying between 50 and 350 m in total thickness (Coqueiro Seco Formation and Rio Pitanga Formation) (Campos Neto et al. 2007). Studies of this formation are often made using outcrops (Tavares et al. 2015; Borghi and Corbett 2013) and cores (Carvalho et al. 2000; Rigueti et al. 2020) that are close analogues of off-shore oil-bearing Pre-salt reservoirs of the Santos (Fm. Itapema; Carlotto et al. 2017) and Campos (Fm. Coqueiros, Carvalho et al. 2000) basins in Brazil.

The term coquina was defined by Schäfer (1972) as a carbonate rock composed of skeletal parts, whose location and composition are governed by the laws of sedimentology rather than biological laws. Coquinas from the Morro do Chaves formation are composed of bivalve shells and ostracodes that originally lived in shallow and oxygenated waters (Azambuja et al. 1998). The shells were subjected to rework and transportation and were deposited on beaches and platforms through storm-induced currents (Carvalho et al. 2000; Teixeira 2012).

Tavares et al. (2015) conducted a facies study at the Atol Quarry, located in São Miguel dos Campos, Alagoas (Fig. 1), in order to understand the composition of the rocks involved. Their study showed a predominance of fragmented shells, without micrite, which were deposited in underwater bars, above the base level of good weather wave action. High shell fragmentation and the absence of micrite would indicate constant rework in a moderate to high energy environment. Whole shell facies with micrite presence were deposited between the base level of good weather and storm wave action. Below the base level of storm wave action, clay deposits occurred under suboxide to anoxic conditions.

Diagenetic actions were the main modifying agents of carbonate rocks. Coquinas of the Morro do Chaves Formation were altered through these processes involving neomorphism, physical and chemical compaction, and micritization (Tavares et al. 2015). These processes impacted directly the pore systems of the rocks, leading to the preservation of primary porosity, the creation of secondary porosity, and pore obliteration. As a consequence, a very heterogeneous porous framework was generated, reflected especially in their permeability (Corbett et al. 2016).

3 Materials and Methods

For our study, we used six plugs (Table 1) taken from core UFRJ 02-SMC-02 drilled in the Atol Quarry (Fig. 2). The cylindrical coquina samples (plugs), having dimensions of 2.5 cm (diameter) versus 5 cm (height), consisted of bioclasts resulting from shell fragmentation of transported lacustrine bivalves and subsequent impact by several stages of diagenesis. Due to these changes, the samples are very complex by containing unusually heterogeneous pore systems.

After plugging, the samples were cleaned to obtain a completely emptied (dried) porous system. For this, we employed the Soxhlet method (McPhee et al. 2015), which is widely used in the oil industry. Possible rock fluids in the coquinas, such as hydrocarbons and salts, were removed using toluene and methanol, respectively. After cleaning, the samples were subjected to oven drying at 60 °C and 40% humidity for a total of 24 h. These

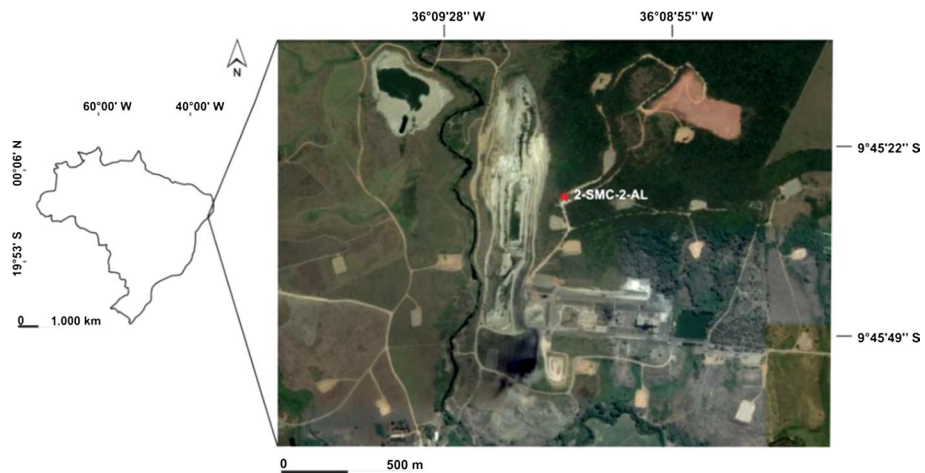
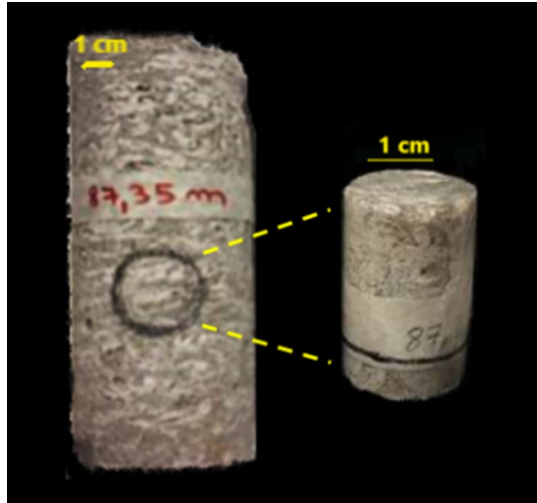


Fig. 1 Location of the Atol Quarry location at São Miguel dos Campos, Alagoas, Brazil

Table 1 Geological descriptions of plugs from the Morro do Chaves Formation

Sample Core depth (m)	Classification	Matrix	Diagenesis	Pore type
87.55	Calcirudite	30% siliciclastic sand. shells	Neomorphism, physical compaction	Interparticle
88.00	Calcirudite	5% siliciclastic sand. Predominance of entire shells	Neomorphism, physical and chemical compaction, dissolution of siliciclastic grains, kaolinite precipitates in secondary pores	Interparticle, moldic
122.45	Calcirudite	1% ostracodes and trace amounts of gastropod. Pre-dominance of entire shells	Neomorphism, physical and chemical compaction, dissolution seams, styloliths	Intraparticle, intercrystalline
136.85	Calcirudite	12% siliciclastic sand	Neomorphism, physical and chemical compaction, kaolinite precipitates in secondary pores	Vugs, moldic
180.00	Calcirudite	Trace amounts of siliciclastic sand and ostracodes	Neomorphism, physical compaction	Vugs, moldic
187.95	Calcirudite	Predominance of entire shells	Neomorphism, physical compaction, dissolution	Vugs, intercrystalline

Fig. 2 Schematic of sample 87.35 (right) taken from core 02-SMC-02 (left). Sample 87.35 contained 30% siliciclastic sand together with predominance of fragmented shells



conditions were used to not degrade possible clays contained within the sample. After drying, the samples were cooled in a desiccator for one hour and then submitted to basic petrophysics experiments.

Routine core analysis is a non-destructive technique used to determine the porosity and permeability as based on Boyle's law and Darcy's law, respectively. Results obtained with a combined gas permeameter–porosimeter (AP-608, from Coretest Systems Inc., Reno, NV) provided a reference for all other petrophysical measurements (McPhee et al. 2015). For the NMR measurements, we saturated the samples in a saline solution consisting of 30,000 ppm KCl brine with a density of 1.0167 g/cm^3 and subjected to a hydrostatic pressure of 138 bar for 24 h (Fig. 3). Even though the coquinas contained very little if any clay, we used brine in part to avoid or limit possible shrink/swell processes (e.g. Ewy 2014). Saturation was confirmed by calculating saturation indexes, whose values were all above 95% indicating satisfactory saturation. The samples were afterwards immersed in a fluid container.

After saturation, the samples were wrapped in Teflon to minimize pore emptying during the NMR measurements. Using a Geospec 2 MHz device (Oxford Instruments) and a Carr-Purcell-Meiboom-Gill (CPMG) pulse sequence (Carr and Purcell 1954), which consists of a 90° radiofrequency pulse followed by a 180° pulse train lagged at $\pi/2$ of the first pulse, echo intensity measurements were taken with a signal-to-noise ratio above 100. Application of inverse Laplace transforms on the data produced time distribution curves of the transverse relaxation (T_2), which were calculated using LithoMetrix™ software from Green Instruments Technology (GreenImaging Techn., Fredericton, NB, Canada). The main parameters of the NMR acquisitions are listed in Table 2.

Because of their destructive nature during the MICP measurements, we removed the rock fragments from the plug surface. The fragments, having a volume of approximately 2 cm^3 , were subjected to a vacuum of 50 to 900 $\mu\text{m Hg}$ inside a penetrometer filled with mercury. Pressure increments were applied, up to a final pressure of 60,000 psi, to obtain accessible pore volumes at different pressures. The data allowed us to estimate pore throat radius distribution curves, and incremental and cumulative porosity amplitudes. The MICP experiments were performed using Micrometrics Auto Pore IV equipment.

Fig. 3 Details of the saturation process of the samples and their storage in brine for subsequent NMR measurements



Table 2 Parameters applied to the NMR experiments

Parameter	Value
Total echos	16,250
Echo time	200 μ s
Number of averages	64
Waiting time between averages	10 s
90° pulse width	12.04 μ s
180° pulse width	24.24 μ s
Temperature	25 °C

The samples were subjected to X-ray microtomography imaging in order to understand the pore framework of the coquinas. Imaging was performed in three sequential steps: acquisition of high-resolution (16-bit) x-ray images using Skyscan model 1173 microtomography, image reconstruction using NRecon[®] software (Skyscan/Bruker, v.1.6.9.4) as detailed by Godoy et al. (2019), and image processing using Avizo Fire[®] 9.5 software (ThermoFisher Scientific, Massachusetts, US). For the acquisition, we used a 1-mm aluminium filter to reduce noise in the images, while the equipment was calibrated with a voltage of 80 kV and 100 μ A. The plugs were rotated 360° with an angular pitch of 0.5°. For the treatment of images, a non-local means filter was used to minimize artefacts and noise caused during acquisition (Lin et al. 2016). One of the steps consisted of segmenting the images, which allows the pores to be identified, and separating them from the sample's mineral framework using the threshold tool (Otsuki et al. 2006; Lore 2018). Threshold values were determined by comparing pixel size with the NMR curves, with T_2 values first being converted to pore radii (Eq. 3). After this, using the auto-skeleton tool (Lore 2018), the segmented pore space was transformed into tubes (made up of sequentially smaller

spheres) and spheres, equivalent to the pore throats and pore bodies, respectively. The output data were used subsequently in the PoreFlow software (Raouf et al. 2013) to assess the digital permeability and to obtain a more complete understanding of the entire pore system and fluid flow within the pore system.

4 Results and Discussion

Results of the core analyses, such as of porosity, permeability, and grain density, as well as the NMR and ADI results for porosity, are presented in Table 3. As can be seen, the samples had porosity values ranging from 8.7 to 16.7% and permeabilities from 8.7 to 245.1 mD. The grain density data reflect a predominance of calcite in the composition of the samples (2.71 g/cm³ in general). The NMR porosity results furthermore show a good correlation with the routine porosity measurements, which suggest that the results were satisfactory and the samples were well saturated. MICP results for the low-permeability samples presented values close to routine porosities, but were lower for the high-permeability samples. This finding can be explained by the pore size in each sample group: generally, the low-permeability samples contained mostly only relatively small pores in the samples used for the measurements, whereas the higher permeability samples had larger pores not present in the fragments used for the porosity.

Figure 4 shows a plot of porosity versus permeability using the routine data. The plot shows data from all samples according to their petrophysical properties, highlighted by two groups: one with a relatively low permeability and the other with a high permeability. Two low-permeability samples had relatively low porosities, and two high-permeability samples had higher porosities, as expected and discussed by Corbett et al. (2016) who noted substantial changes in permeability with only slight changes in the porosity. However, two samples (122.45 and 187.95) had nearly the same porosity but showed a large difference in their permeability (to be discussed later).

Figure 5 shows the pore size distributions as a function of the relaxation time using five size partitions as employed by Silva et al. (2015). The curves show considerable heterogeneity among the samples, consistent with the variability in the permeability versus porosity relationships shown in Fig. 4. The pore partitions of Silva et al. (2015), consisted of micropores (T_2 values up to 1 ms), a transition from micropores and mesopores (from 1 to 10 ms), mesopores (10 to 100 ms), a transition from mesopores to macropores (100 to 1000 ms), and macropores (above 1000 ms). As indicated by Gonçalves et al. (2017), it is not surprising that most partitions actually contributed to the flow process in our study

Table 3 Estimated sample hydraulic parameter values using core analyses, NMR, and MICP

Sample core depth (m)	ρ_{grains} (g/cm ³)	ϕ_{routine} (%)	K_{routine} (mD)	ϕ_{NMR} (%)	ϕ_{MICP} (%)
87.35	2.70	10.2	5.25	9.4	9.3
88.00	2.71	8.7	5.21	9.0	8.3
122.45	2.72	12.3	5.65	12.1	12.3
136.85	2.71	16.0	245.0	15.1	10
180.00	2.71	16.7	245.1	16.3	13.2
187.95	2.70	12.2	152.4	12.4	8

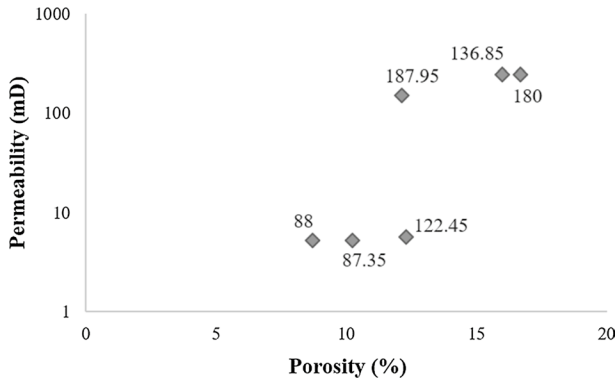


Fig. 4 Plot of permeability versus porosity for six core samples. The plot shows a non-unique relationship between permeability and porosity. Samples 187.95 and 122.45 had similar porosity but different permeabilities, while samples 88, 87.35, and 122.45 had similar permeabilities but different porosities

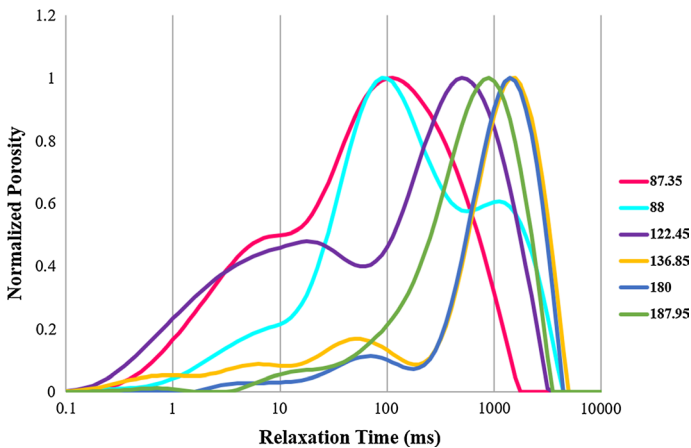


Fig. 5 Plot of the relaxation time for different samples using a five-partition approximation. Curves are mostly non-overlapping, indicating that the samples are heterogeneous. This is consistent with variations in the permeability and porosity values of the samples shown in Fig. 4

since carbonate rocks are known to have pore sizes that generally vary over three orders of magnitude. Based on this information, we note that samples 87.35 and 88, which have a lower permeability, show a bimodal distribution, with most of the pores being in the mesoporous region. On the other hand, sample 122.45 had a very well-defined bimodal distribution, but with a predominance of macropores. Of the high-permeability samples, sample 187.95 had a remarkable unimodal distribution at or near the macroporosity region. This demonstrates that even having the same porosity as sample 122.45, its permeability is linked more to the pore throats, which are responsible for flow through the porous space. Samples 136.85 and 187.95 did have very similar distributions, demonstrating their petrophysical similarity.

The MICP measurements produced curves of the capillary pressure as a function of mercury saturation, from which pore size distributions could be extracted (Moctezuma

et al. 2004). Figure 6 shows that some variability is apparent between the measured capillary–saturation curves. The curves show an increase in capillary pressure consistent with mercury entry into pores having increasingly smaller diameters. Samples 87.35, 88 and 122.45 show that 30% of the pores were already accessed with pressures up to 10 psi, thus characterizing the larger pore throat apertures. About 70% of the pores in these samples were intruded at a pressure of 100 psi, while the smallest pores making up 15% of the total were intruded with higher pressures. Knowing that these samples have lower porosities and permeabilities, one can understand that their pore space is interconnected by means of narrow throats.

For samples with a higher porosity and permeability, different capillary pressure curves were obtained. For example, sample 136.85 required slightly higher pressures throughout the mercury intrusion test. This indicates that even with smaller pores, the sample had good connectivity among the pores, thus contributing to flow in the sample. Sample 187.95 showed that around 60% of its pores were intruded with pressures up to 20 psi, which suggests that these pores had relatively large throats. To access the remaining pore space, a progressive increase was required, which caused a difference in the slope of the curve, reflected by a reduction in the pore throats. Sample 180 differed in this respect from the others: 70% of its pores were accessed with pressures up to 20 psi, characterizing pores with large throats. The remaining pores were accessed using higher pressures, characterized by the slope of the curve. The low-permeability samples, for the most part, hence had similarities in terms of pore throat size due to the slight increase in capillary pressures, with a considerable increase occurring in only a small pore fraction. High-permeability levels presented differences in the intrusion pressures, demonstrating that although the samples had similar permeabilities, they contained a different pore network structure.

Transformations of the T_2 distributions to pore size were carried out by overlapping the NMR curve over the MICP curve and shifting it so that the two peaks of two curves overlap (Mesquita et al. 2016; Zhang and Hebing 2014). Once visually verified that both distributions (i.e. of mercury saturation and T_2) correlated well, we adjusted ρ_2 in Eq. (3) until the distributions had the same maximum, as can be seen in Fig. 7. Sometimes, it is necessary to move the peaks away to obtain the same end points for the two curves (as seen for samples 122.45 and 187.95). While this is an approximation, the approach has been found

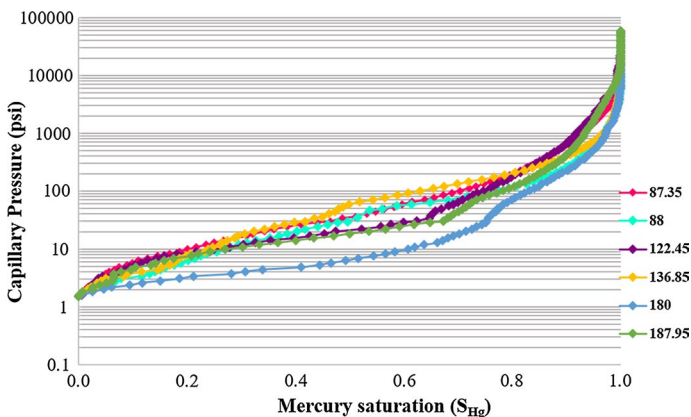


Fig. 6 Plot of the MICP measurements used to calculate capillary pressure curves as a function of mercury saturation

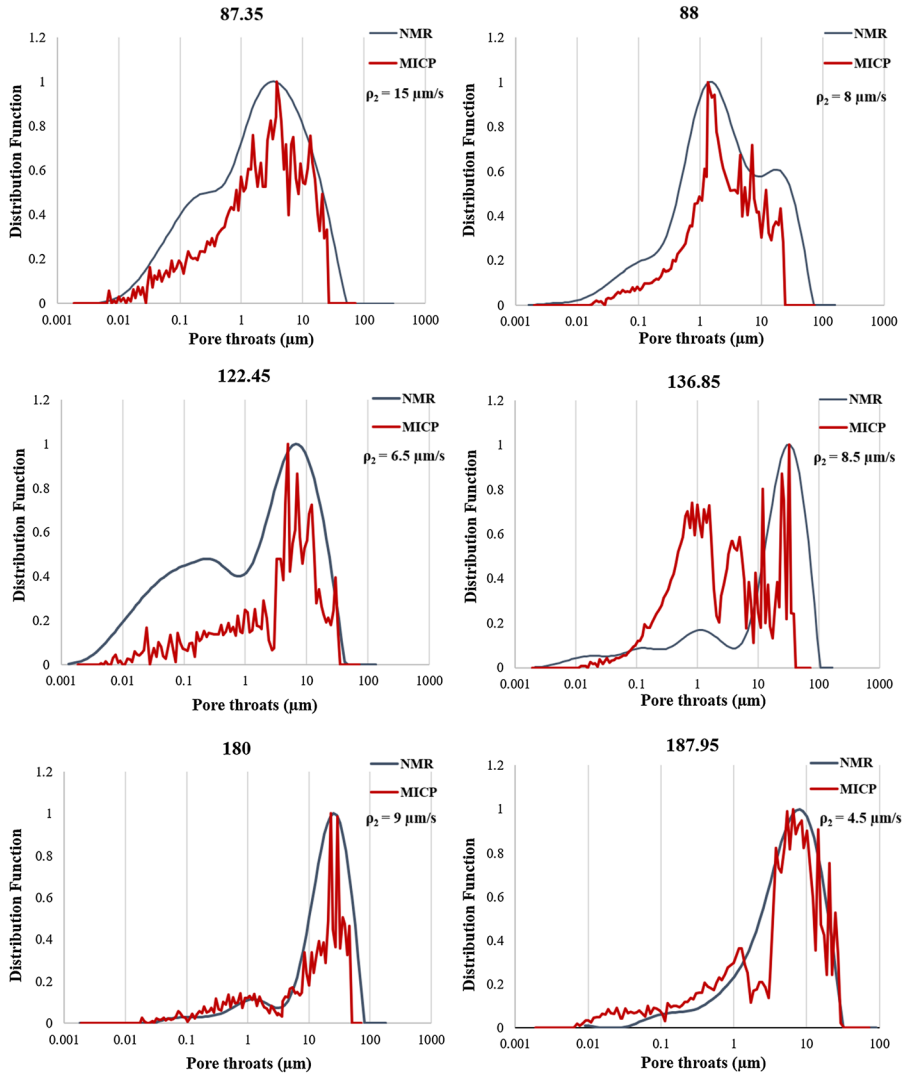


Fig. 7 Fitting of the NMR and MICP curves

to provide accurate permeability values for modelling applications (Mesquita et al. 2016; Rios et al. 2016; Souza et al. 2013). Yet, because of the complexity of the samples, a better option is to simply perform a visual fitting in which the micropores from MICP are combined with the NMR results, and so on. Samples 87.35, 88, 122.45, 180 and 187.95 generated very reasonable fits for NMR and MICP curves, which visually appear quite similar. The distributions suggest that the pore throats merged slowly with the main channels in the permeable part of the system (Basan et al. 1997). In contrast, sample 136.85 showed important differences between the two curves. The NMR curve exhibited a triple porosity distribution dominated very much by the larger pores. By contrast the triple porosity MICP

curve is predominated mostly by mesoporosity. Knowing that MICP is sensitive mostly only to the throats and NMR to the entire pore space, the sample seems typical of a situation where the larger pores are surrounded by smaller pores, with MICP assigning volumes first to the smaller pores since the larger pores are invaded by mercury only after invasion of the smaller pores. The complexity of sample 136.85 is a common characteristic of carbonate rocks. Sample 122.45 is similarly interesting in that the NMR curve shows a higher percentage of pores in the micropore and mesopore regions as compared to the throats in the MICP curve. We conclude that the pores of this sample must have relatively better connections, relative to the other samples. As noted earlier, the NMR curve of sample 136.85 had most of its pores within the meso-/macro-region, while the MICP curve showed a triple porosity system with a predominance of mesopores. Figure 7 further contains important information about the surface relaxativity, ρ_2 . The range of values of ρ_2 we obtained (between 6.5 and 15 $\mu\text{m/s}$) is very typical of carbonate rocks.

For the pore radius distributions, we used thresholds based on the percentage of visible pores at the given resolution, as developed by Hoerlle et al. (2018). After segmentation, the connected pores were transformed into cylindrical pore throats and spherical pore bodies using the skeletonization tool, resulting in a series of nodal points, segments, and nodes that served as input to calculate porosity and permeability of the sample using PoreFlow software (Raouf et al. 2013). Considering routine core analysis as a calibration technique (McPhee et al. 2015), PoreFlow results showed a good agreement with the measurements (provides shown in Table 4). While the porosities obtained with PoreFlow were smaller, the calculated and measured permeabilities were similar for most samples. This is further shown in Fig. 8, which indicates excellent agreement between the PoreFlow predictions and the routine measurements, well within a factor of 3 generally considered acceptable for permeability estimations using NMR (e.g. Kenyon et al. 1988). We hence conclude that the pore system observed at this resolution was responsible for flow within the samples as simulated.

Table 3 showed that samples 122.45 and 187.95 had the same porosity (12%) but different permeability values (5.65 and 152.4 mD, respectively). To better understand this difference, PoreFlow was used to simulate fluid flow within the pore topologies of these two samples. All image components were analysed for pore connectivities using Paraview (Ayachit 2015), with results shown in Fig. 9. The images display the connected pores responsible for the permeability of the samples. Figure 9a–b shows the pore clusters of sample 122.45, with each cluster having a different colour to indicate a set of connected pores. In total, 1748 pore clusters were recognized. Figure 9b shows the largest pore cluster

Table 4 Comparison of porosities and permeabilities obtained with the routine core analyses and calculated using PoreFlow

Samples core depth (m)	ϕ_{routine} (%)	ϕ_{PoreFlow} (%)	K_{routine} (mD)	K_{PoreFlow} (mD)
87.35	10.2	8.1	4.57	4.58
88.00	8.7	6.1	5.21	4.4
122.45	12.3	4.2	5.65	3.7
136.85	16.7	13.2	245	249.2
180.00	16.7	10.8	245.1	236.7
187.95	12.2	6.8	152.4	138.9

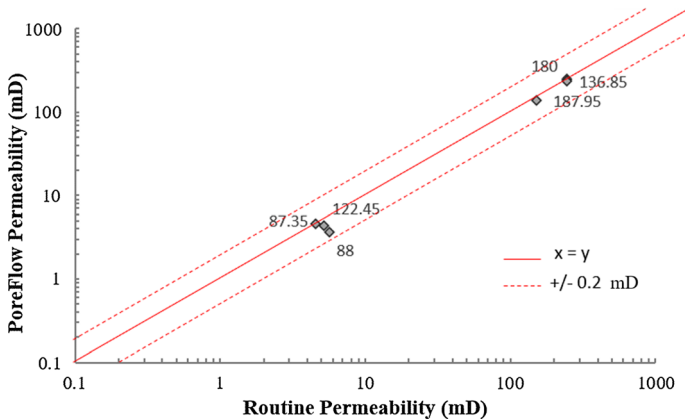


Fig. 8 Plot comparing the routine permeability measurements with the PoreFlow predictions

responsible for most of the fluid flow through the entire sample. Figure 9c–d shows similar results for sample 187.95, with Fig. 9c exhibiting as much as 724 distinct (i.e. separate from each other) pore clusters making up the pore network of the rock. The different makeup of the two main percolating clusters in Fig. 9 is a reflection of the different volume of connecting pores of the two samples and their impacts on the permeability: sample 122.45 had a smaller percolating cluster with a lower volume of pores and consequently a lower permeability, while sample 187.95 had a much higher volume of connecting pores pertaining to the main cluster, leading to a much higher permeability. The large fraction of non-percolating clusters in sample 122.45 (Fig. 9a) must have been responsible for the deviation between the NMR and MICP curves for this samples as shown in Fig. 7. While NMR captures the entire pore system, the MICP measurements are more likely affected by the presence of complex non-percolating pore clusters since this method is based on the flow of mercury into the sample. Similar correlations for other images were found to be useful for explaining why certain samples with similar total porosity provided different permeability values. As explained well by Lucia (1999), diagenesis typically reduces porosity, redistributes the pore space, and alters the prevailing permeability and capillary characteristics. The resulting rock alterations may well have caused most or all of the permeability modifications and pore complexities of our samples.

The connectivity data of each pore body were also analysed in terms of the overall pore network of samples 122.45 and 187.95. The coordination number of the pores (also called pore connectivity) represents the average number of pore bodies which are connected with adjacent pores (Sahimi et al. 2012; Raoof and Hassanizadeh 2010). This parameter is a fundamental feature of pore networks and has a noticeable impact on calculations of the hydraulic conductance of porous rocks (Chen et al. 2003; Vasilyev et al. 2012). Figure 10 provides a comparison of the coordination numbers of the same two samples (i.e. of 122.45 and 187.95) obtained with the Avizo[®] software. Sample 187.95 has much higher counting bins, especially when looking at three coordination numbers, than coquina 187.95. This implies a much better pore continuity and hence a higher permeabilities of sample 187.95 at the same porosity.

Another way to explain the permeability differences is through a pore body-throat analysis. Using the skeleton of the microCT images, one can quantify the volume and

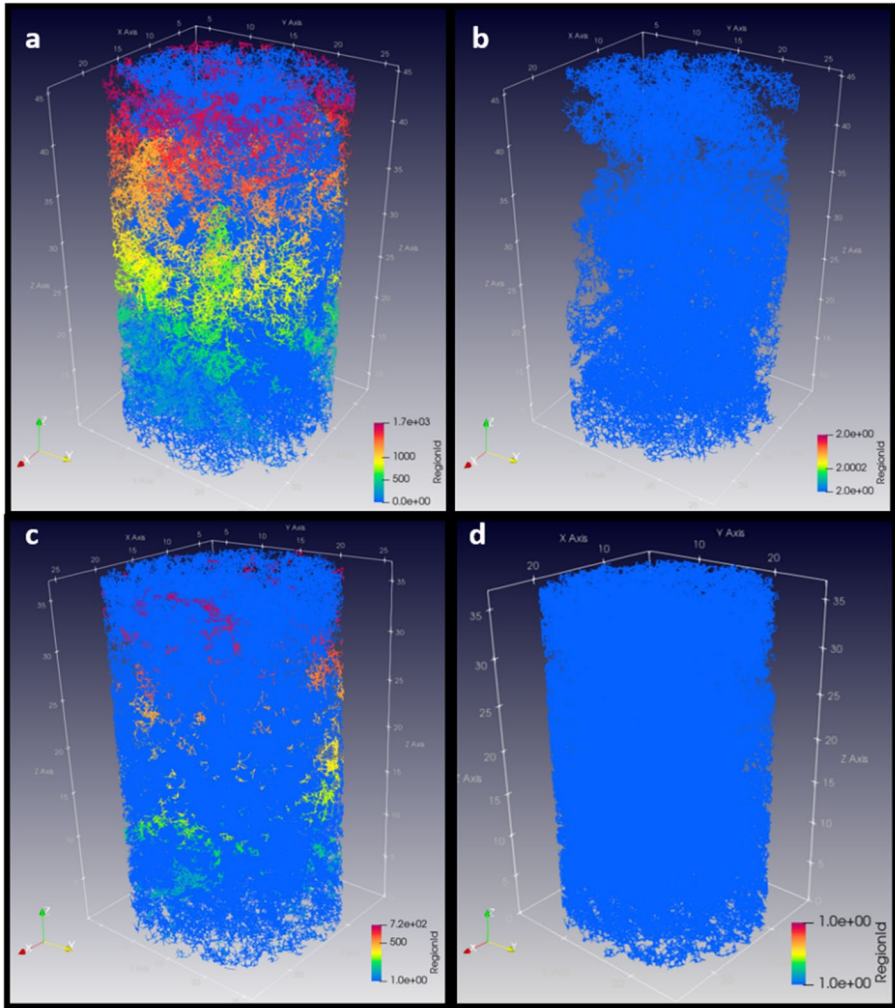


Fig. 9 Distribution of pore clusters in two rock samples: a) all pore clusters in sample 122.45 and b) its main pore cluster responsible for flow through the sample and its permeability; c) all pore clusters of sample 187.95 and d) its main pore cluster. This figure explains why sample 187.95 with a similar porosity as sample 122.45 has a much higher permeability (as indicated in Fig. 4)

size of these elements, which in their totality should be a reflectance of the complexity of the pore space of the rocks. Figure 11 exhibits the pore throat and pore body distributions of samples 122.45 and 187.95. The plots show that sample 187.95 had larger element volumes, which is consistent with its higher permeability compared to sample 122.45. Regarding the pore sizes obtained from the images, the microCT values were higher than those determined by NMR using the MICP match. A comparison of these two techniques assumes equivalence between the pore body and pore throat sizes, which may not be appropriate for heterogeneous carbonate samples. Still, using

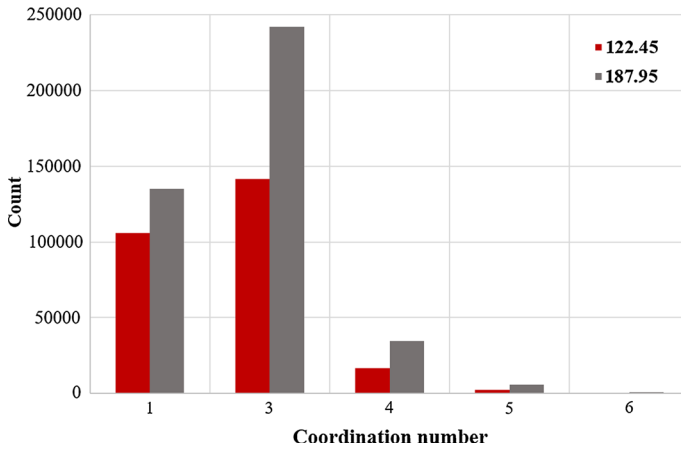


Fig. 10 Comparison of the distribution of coordination numbers for samples 122.45 and 187.95

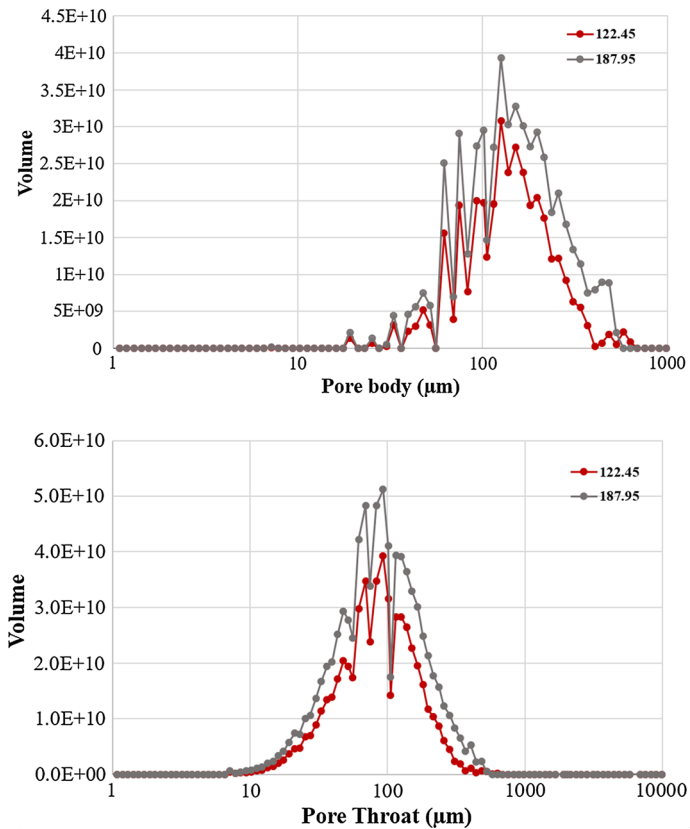


Fig. 11 Comparison of the pore bodies and pore throats of samples 122.45 and 187.95

this conversion, the permeability as determined from the images was satisfactory, thus confirming applicability of the technique.

We noticed that the pore throats found in the samples using microCT images had values higher than those determined using MICP. As mentioned before, MICP results are based on the Washburn equation (Washburn 1921), which approximates the porous system as a bundle of cylindrical tubes. When analysing carbonate rocks (especially coquinas), one must consider heterogeneity in the pore systems in terms of different pore shapes. The images in Fig. 12 show difference between the pore systems of two samples. Although the images are in two dimensions (XY slices from microCT), it is possible to recognize that the intraparticle pores of sample 122.45 are different from the larger vugs of sample 187.95. To better understand these pores, our next step was to scan the samples with higher resolution (3 μm) in order to observe the resolution impact on unresolved pore throats.

Finally, we note that surface relaxativity, ρ_2 , may be a complicating factor for this study. Since ρ_2 does not have an exact form of calculation but only provides approximations, this parameter generally is subject to much uncertainty, also in our study. Another factor that influences the NMR results is the bulk effect on the larger pores. Above 2.5 s (the saturating fluid relaxation time of the samples), the spins no longer completely collide with the pore walls of the pore network inside the sample, which may cause the measured relaxation time to be less reliable (Kenyon 1997). This causes uncertainty in the size of especially the larger pores.

5 Concluding Remarks

This study focused on the effects of pore structure, pore size distribution, and connectivity to better understand why significant permeability variations occur in carbonate rock samples having similar porosity values. Routine core analyses, NMR and MICP studies were performed on coquinas samples from the Morro do Chaves Formation, which is considered a close analogue of Brazilian pre-salt oil reservoirs. Integration of the various methods produced estimates of the surface relaxativity needed to transform relaxation times into

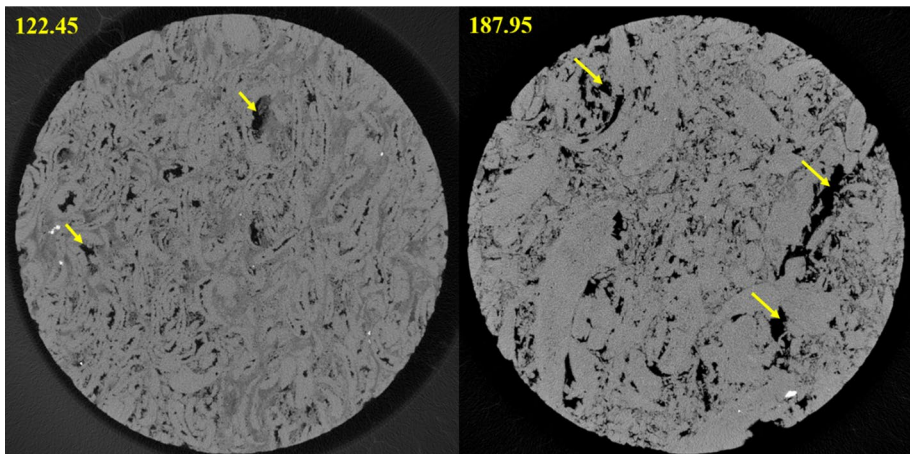


Fig. 12 2D slices from microCT highlighting pore type

the pore size distribution. Threshold values of the distributions, based on the percentage of visible pores at a given resolution, were used (maximum porosity visible in the resolution), considering the pore radius distribution. The microCT images were used to obtain the skeleton, which in turn provided necessary input data (points, segments, and nodes) for porosity and permeability calculations using the PoreFlow software.

Calculated permeabilities showed excellent agreement with routine laboratory measurements. Differences in the permeability of two coquinas having the same porosity could be explained using image analysis and statistical correlations, as well as by considering pore connectivity. Samples having pore bodies with higher coordination numbers showed much larger permeabilities at similar porosities. A pore body-throat analysis could also explain some of the permeability differences. The increase in permeability is related to the presence of larger elements within the connecting pore system. Although the range of pore bodies and pore throats observed on microCT images were higher than determined by NMR using a MICP match, some aspects may need consideration. For example, when combining NMR and MICP, an equivalence is assumed between the pore body to pore throat ratio, which is not necessarily very realistic for carbonate rocks. Pore throats determined using microCT showed differences with those of the MICP experiments. The manner in which pressure is converted to pore radius may present for this reason also some uncertainty for the carbonate rocks. Inaccurate or incomplete definition of some of the NMR parameters, notably surface relaxativity and bulk effects, may also introduce some uncertainty for especially the larger pores.

Our study in this paper focused on the micro-scale petrophysical properties of relatively complex samples (coquinas). While macro-scale multi-phase reservoir simulations depend on having petrophysical properties that are reliable at the larger scale, they still must be as consistent as possible with the micro-scale physical measurements. Required properties include porosity, absolute and relative permeabilities (the latter as a function of fluid saturation), contact angles, and various geochemical parameters. They are needed for effective characterization of carbonate rock formations, including their micro-scale and macro-scale heterogeneities. These issues are especially important for carbonate oil reservoirs in the Brazilian pre-salt, which are unusually heterogeneous as characterized by a broad spread in their pore size distributions due to the presence of vugs and even larger pores of different sizes. Vuggy carbonates are particularly challenging to characterize in terms of relevant bi- or multi-modal petrophysical properties.

Permeability is one of the key parameters for reservoir assessments and management. Direct measurements of permeability require laboratory analyses of drilled reservoir cores. NMR logging provides indirect in situ permeability data, which could be used along with various semi-empirical equations to estimate permeability from the measured porosity values. Unfortunately, current permeability models are based on assumptions that often do not apply to carbonate rocks, such as having a well-connected pore system. Chemical and biological processes during diagenesis of carbonate rocks typically cause a profound reorganization of the initial pore structure, leading to a broad range of pore types and sizes. Our rock samples have clearly shown that samples with different porosities can have similar permeability values. This shows that, for such complex samples, Kozeny–Carman-type relations are not adequate because they assume a unique relation between porosity and permeability. We expect that more complex relations which include topological properties of the media should be developed (Parvan et al. 2020).

Another point to consider is how different techniques with their different results can contribute to a better understanding of complex rocks. Routine core results are important since they provide a calibration for judging other techniques. NMR in principle gives

exceptionally good results for porosity and the pore size distribution. Still, several aspects are important in terms of field applications. One aspect relates to measurements that can be done via a well, during logging, to estimate permeabilities. If the measurements can be made through the well itself and in the laboratory, this would become a preferred method in petrophysics. MICP (at first developed to obtain porosities of irregular samples) leads to porosities and estimates of the permeability from the obtained pore throat distribution consistent with the imposed boundary conditions. Using microCT images, numerical simulations can be done also to determine porosities and permeabilities. In this case, the resolution will guide all the results to be obtained. The most powerful asset of the latter technique is its ability to carefully observe the pore system, while the other tools deliver more global values without direct visualization. We conclude that many available techniques are potentially important to obtain relevant information about a certain rock formation, and hence, that integration of the various techniques and their results will optimize our understanding about the complex pore system involved.

Finally, we note that pore-scale modelling and upscaling based on its results is key for reliable characterization of strongly heterogeneous carbonate rock formations, which typically have representative elementary volumes (REV's) that are far too large for direct numerical simulations. Correct upscaling must focus on those aspects of the system that are controlling fluid flow and/or contaminant transport at the relevant scale. Pore network modelling (PNM) is one approach to speed up simulations of large porous systems since flow and transport in very large samples can be simulated, which generally is not feasible using direct numerical solutions, especially under common multi-phase flow conditions. In this study, we attempted to understand and describe the interplay between porosity and absolute permeability of heterogeneous carbonates at the pore scale and use PoreFlow to simulate fluid flow through the sample to drive the hydraulic properties. Having accurate pore structures, PoreFlow can be used to derive more complex constitutive relationships such as those between saturation and relative permeability as well as capillary pressure (Raouf and Hassanizadeh 2012). A well-integrated methodology is needed to allow pore network modelling up to REV's for use at the larger scale. The methodology presented in this paper, combined with improved analytical correlations between porosity and permeability, may facilitate more realistic representations of the continuum scale.

Acknowledgments This research was carried out in association with the ongoing R&D projects registered as ANP 19027-2, “Desenvolvimento de infraestrutura para pesquisa e desenvolvimento em recuperação avançada de óleo – EOR no Brasil” (UFRJ/Shell Brasil/ANP) setting up a advanced EOR Laboratory facility for R&D in Brasil, and ANP 20163-2, “Análise experimental da recuperação de petróleo para as rochas carbonáticas do pré-sal brasileiro através da injeção alternada de CO₂ e água”, with samples provided by Project SACL (Análise geológica sedimentar de sucessões carbonáticas do Cretáceo em uma bacia sedimentar brasileira (ANP n.18993-6), all sponsored by Shell Brasil under the ANP R&D levy as “Compromisso de Investimentos com Pesquisa e Desenvolvimento”. This study was financed in part by the Coordenação de Aperfeiçoamento de Pessoal de Nível Superior- Brasil (CAPES)—Finance Code 001, and carried out with the support of CNPq, National Council of Scientific and Technological Development—Brazil. We acknowledge Professor Rodrigo Bagueira (UFF-LAR) for helping with saturating the samples and use of the NMR equipment. We also thank the research teams of LRAP/COPPE/UFRJ and LAGESED/UFRJ.

Open Access This article is licensed under a Creative Commons Attribution 4.0 International License, which permits use, sharing, adaptation, distribution and reproduction in any medium or format, as long as you give appropriate credit to the original author(s) and the source, provide a link to the Creative Commons licence, and indicate if changes were made. The images or other third party material in this article are included in the article's Creative Commons licence, unless indicated otherwise in a credit line to the material. If material is not included in the article's Creative Commons licence and your intended use is not permitted by statutory regulation or exceeds the permitted use, you will need to obtain permission directly from the copyright holder. To view a copy of this licence, visit <http://creativecommons.org/licenses/by/4.0/>.

References

- Ayachit, U.: The Paraview guide: A Parallel Visualization Application. Kitware Inc, New York (2015)
- Azambuja, N.C., Arienti, L.M., Cruz, F.E.: Guidebook to the rift-drift Sergipe-Alagoas passive margin basin, Brazil. In: AAPG Int. Conf. and Exhibition. AAPG, Rio de Janeiro, Brazil, p. 113 (1998)
- Basan, P.B.; Lowden, B.D.; Whattler, P.R.; Attard, J.J (1997): Pore-size data in petrophysics: a perspective on the measurement of pore geometry. In: Lovell, M.A., Harvey, P.K. (eds.) Developments in Petrophysics, Geological Society of London, Special Publ. 122, p. 47–67 (1997). <https://doi.org/10.1144/gsl.sp.1997.122.01.05>
- Borghi, L.; Corbett, P.W.M. (2013): Lacustrine carbonates For the purpose of reservoir characterization: Are they different? Offshore Techn. Conf., Rio de Janeiro, Brazil (2013). <https://doi.org/10.4043/24482-ms>
- Brown, A.A.: Interpretation permeability from mercury injection capillary pressure data. In: AAPG 2015 Annual Convention and Exhibition, Colorado (2015)
- Buttler, J.P., Reeds, J.A., Dawson, S.V.: Estimating solution of first kind integral equations with non-negative constraints and optimal smoothing. Siam J. Numer. Anal. (1981). <https://doi.org/10.1137/0718025>
- Carr, H.Y., Purcell, E.M.: Effects of diffusion on free precession in nuclear magnetic resonance experiments. Phys. Rev. **94**(3), 630 (1954)
- Carlotto, M.A., Da Silva, R.C.B., Yamato, A.A.: Libra: A newborn giant in the Brazilian Presalt Province. In: Merrill, R.K., Sternbach, C.A. (eds.) Giant Fields of the Decade 2000–2010: AAPG Memoir **113**, 165–176 (2017). <http://doi.org/10.1306/13572006M1133685>
- Carvalho, M.D., Praça, U.M., Telles, A.C.S.: Bioclastic carbonate lacustrine facies models in the Campos basin (Lower Cretaceous), Brazil. In: Gierlowski–Kordesch, E.H., Kelts, K.R. (eds.) Lake Basins Through Space and Time: AAPG Studies in Geology 46, pp.245–256 (2000)
- Chang, C.T.P., Choi, C., Hollenshead, J.T., Michalak, R., Phan, J., Saavedra, R., Slattery, J.C., Uh, J., Valestrand, R., Watson, A.T., Xue, S.: NMR characterizations of properties of heterogeneous media. Final Report, Texas Engineering Experiment Station (TEES) (2004) <http://doi.org/10.2172/838814>
- Chen, S.C., Lee, E.K., Chang, Y.I.: Effect of the coordination number of the pore-network on the transport and deposition of particles in porous media. Sep Purif Technol. (2003). [https://doi.org/10.1016/S1383-5866\(02\)00096-5](https://doi.org/10.1016/S1383-5866(02)00096-5)
- Chi, L., Heidari, Z.: Directional-permeability assessment in formations with complex pore geometry with a new NMR based permeability model. Soc Pet. Eng. J. **21**(04), 1–436 (2016)
- Cnudde, V., Boone, M.N.: High-resolution X-ray computed tomography in geosciences: a review of the current technology and applications. Earth Sci. Rev. (2013). <https://doi.org/10.1016/j.earscirev.2013.04.003>
- Corbett, P.W.M., Estrella, R., Shoier, A., Morales, A., Borghi, L.: Integration of cretaceous Morro do Chaves rock properties (NE Brazil) with the Holocene Hamelin Coquina architecture (Shark Bay, Western Australia) to model effective permeability. Pet. Geosci (2016). <https://doi.org/10.1144/petgeo2015-054>
- de Sergipe-Alagoas, B.: Campos Neto, O.P.A., Souza-Lima, W., Cruz, F.E.G. Boletim de Geociências da Petrobrás **15**, 405–415 (2007)
- de Vries, E.T., Raoof, A., van Genuchten, MTh: Multiscale modelling of dual-porosity porous media: a computational pore-scale study for flow and solute transport. Adv. Water Resour. (2017). <https://doi.org/10.1016/j.advwatres.2017.04.013>
- Dernaika, M., Al Mansoori, M., Singh, M., Al Dayyani, T., Kalam, Z., Bhakta, R., Koronfol, S., Uddin, Y.N.: Digital and conventional techniques to study permeability heterogeneity in complex carbonate rocks. Petrophys **59**, 373–396 (2018)
- Dong, H., Blunt, M.J.: Pore-networking extraction from micro-computerized tomography images. Phys. Rev. (2009). <https://doi.org/10.1103/PhysRevE.80.036307>
- Ewy, R.T.: Shale swelling/shrinkage and water content change due to imposed suction and due to direct brine contact. Acta Geotech. **9**, 869–886 (2014). <https://doi.org/10.1007/s11440-013-0297-5>
- Feijó, F.J., Vieira, F.A.B.: Sequências Cretácicas das Bacias de Sergipe e Alagoas. São Paulo. Geociências **10**, 153–168 (1991)
- Fleury, M., Romero-Sarmiento, M.: Characterization of shales using T_1 – T_2 NMR maps. J Pet Sci Eng. **137**, 55–62 (2016). <https://doi.org/10.1016/j.petrol.2015.11.006>
- Godoy, W., Pontedeiro, E.M., Hoerlle, F., Raoof, F., van Genuchten, M.T., Santiago, J., Couto, P.: Computational and experimental pore-scale studies of carbonate rock sample. J. Hydrol. Hydromech. (2019). <https://doi.org/10.2478/johh-2019-0009>

- Gonçalves, E.C., Silva, P.N., Silveira, C.S., Carneiro, G., Domingues, A.B., Moss, A., Pritchard, T., Plastino, A., Azeredo, R.B.V.: Prediction of carbonate rock type from NMR responded using data mining techniques. *J. Appl. Geophys.* (2017). <https://doi.org/10.1016/j.jappgeo.2017.03.014>
- Gundogar, A.S., Ross, C.M., Akin, S., Kovscek, A.R.: Multiscale pore structure characterization of Middle East carbonates. *J. Pet. Sci. Eng.* (2016). <https://doi.org/10.1016/j.petrol.2016.07.018>
- Hoerlle, F., Rios, E.H., Silva, W.G.A.L., Pontedeiro, E.M.B.D., Lima, M.C.O., Corbett, P.W.M., Alves, J.L.D., Couto, P.: Nuclear magnetic resonance to characterize the pore system of coquinas from Morro do Chaves Formation, Sergipe-Alagoas basin, Brazil. *Revista Brasileira de Geofísica* (2018). <https://doi.org/10.22564/rbgf.v36i3.1960>
- Jin, X., Yu, C., Liu, X., Li, J., Jiao, H., Su, L.: Multi-scale digital rock quantitative evaluation technology on complex reservoirs. In: SPE Asia Pacific Oil & Gas Conference & Exhibition, Australia (2018). <https://doi.org/10.2118/191878-18apog-ms>
- Kaufmann, J.: Characterization of pore space of cement-based materials by combined mercury and Wood's metal intrusion. *J. Am. Ceram. Soc.* (2009). <https://doi.org/10.1111/j.1551-2916.2008.02834.x>
- Kenyon, W.E., Day, P.I., Straley, C., Willemsen, J.F.: A three-part study of NMR longitudinal relaxation properties of water-saturated sandstones. *Soc. Pet. Eng. J.* **3**(03), 622–636 (1988)
- Kenyon, W.: Petrophysical principles of applications of NMR logging. *Log Anal.* **38**, 21–43 (1997)
- Li, A., Ding, W.L., Wang, R.Y., He, J.H., Wang, X.H., Sun, Y.X., Gu, Y., Jiao, N.L.: Petrophysical characterization of shale reservoir based on nuclear magnetic resonance (NMR) experiment: a case study of lower Cambrian Qiongzhusi formation in eastern Yunnan Province, South China. *J. Nat Gas Sci Eng* (2017). <https://doi.org/10.1016/j.jngse.2016.11.034>
- Lima, M.C.O., Martins, L.P., Rios, E.H., Boyd, A., Pontedeiro, E.M.B.D., Hoerlle, F., Lipovetsky, T., Neto, A.O., Mendes, M., Borghi, L.F., Couto, P (2019) Rock typing of coquinas from the Morro do Chaves Formation. In: 16th Int Congress Brazilian Geophysical Society, Rio de Janeiro (2019). <https://doi.org/10.22564/16cisbgf2019.290>
- Lin, Q., Al-Khulaifi, Y., Blunt, M.J., Bijeljic, B.: Quantification of sub-resolution porosity in carbonates rocks by applying high-salinity contrast brine using X-ray microtomography differential imaging. *Adv. Water Resour.* (2016). <https://doi.org/10.1016/j.advwatres.2016.08.002>
- Lore, C. Thermo Scientific™ Avizo™ Software 9. <https://assets.thermofisher.com/TFS-Assets/MSD/Product-Guides/user-guide-avizo-software.pdf>. Accessed 15 January
- Lucia, F.J.: Characterization of petrophysical flow units in carbonate reservoirs: discussion 1. *AAPG Bull.* (1999). <https://doi.org/10.1306/E4FD2EA1-1732-11D7-8645000102C1865D>
- McPhee, C., Reed, J., Zubizarreta, I. (Eds.): Core sample preparation. In: *Core Analysis: A best Practice Guide*, pp. 138–143. Elsevier, Amsterdam (2015)
- Mesquita, P. V., Azeredo, R. B. V., Rios, E. H., Souza A. A. Silva, B. A. C., Faria, B. M., Boyd, A.: NMR-MICP Integration and Permeability: A new free petrophysics software, IBP. In: *Rio Oil and Gas Expo & Conference IBP-1370-16*. (2016)
- Moctezuma-Berthier, A., Vizika, O., Thovert, J.F., Adler, P.M.: One- and two-phase permeabilities of vugular porous media. *Transp. Porous Media* **56**, 225–244 (2004)
- Mostaghimi, P., Blunt, M.J., Bijeljic, B.: Computations of absolute permeability on micro-ct images. *Math. Geosci.* (2013). <https://doi.org/10.1007/s11004-012-9431-4>
- Oliveira, G., Ceia, M., Missagia, R., Neto, I.L., Santos, V.: 2-D image parameters to predict permeability in carbonate rocks. *SEG Tech. Progr. Expand. Abstr.* (2019). <https://doi.org/10.1190/segam2019-3216906.1>
- Otsuki, B., Takemoto, M., Fujibayashi, S., Neo, M., Kokubo, T., Nakamura, T.: Pore throat size and connectivity determine bone and tissue ingrowth into porous implants: three-dimensional micro-CT based structural analyses of porous bioactive titanium implants. *Biomaterials* (2006). <https://doi.org/10.1016/j.biomaterials.2006.08.013>
- Parvan, A., Jafari, S., Rahnama, M., Raouf, A.: Insight into particle retention and clogging in porous media; a pore scale study using lattice Boltzmann method. *Adv. Water Resour.* **138**, 103530 (2020). <https://doi.org/10.1016/j.advwatres.2020.103530>
- Purcell, W.R.: Capillary pressures—their measurement using mercury and the calculation of permeability therefrom. *Pet. Trans.* (1949). <https://doi.org/10.2118/949039-G>
- Raouf, A., Hassanizadeh, S.M.: A new method for generating pore-network models of porous media. *Vadose Zone J.* (2010). <https://doi.org/10.1007/s11242-009-9412-3>
- Raouf, A., Hassanizadeh, S.M.: A new formulation for pore-networking modelling of two-phase flow. *Water Resour. Res.* **48**(1), 1514 (2012)
- Raouf, A., Nick, H.M., Hassanizadeh, S.M., Spiers, C.J.: Pore-scale modelling of reactive transport in well-bore cement under CO₂ storage conditions. *Int. J. Greenh. Gas Control* **11**, S67–S77 (2012)

- Raouf, A., Nick, H.M., Hassanizadeh, S.M., Spiers, C.J.: PoreFlow: a complex pore-network model for simulation of reactive transport in variably saturated porous media. *J. Comp. Geosci.* (2013). <https://doi.org/10.1016/j.cageo.2013.08.005>
- Ravlo, V., Bhattad, P., Knackstedt, M., Plant, L.: Using digital rock technology for multi-scale reservoir characterization. *Gulf Coast Assoc. Geol. Soc. Trans.* **66**, 859–863 (2016)
- Riguetti, A.L., Dal'Bó, P.F., L, Borghi, Mendes, M.: Bioclastic accumulation in a lake rift basin: the early cretaceous coquinas of the Sergipe-Alagoas basin Brazil. *J Sedim Res* (2020). <https://doi.org/10.2110/jsr.2020.11>
- Rios, E.H., Figueiredo, I., Muhammed, A., Azeredo, R. B. V., Moss, A., Pritchard, T., Glassborow, B.: NMR permeability estimators under different relaxation time selections: a laboratory study of cretaceous diagenetic chalks, SPWLA. In: 55th Annual Logging Symposium (2014)
- Sahimi, M.: *Flow and Transport in Porous Media and Fractured Rock: from Classical Methods to Modern Approaches*. Wiley, Germany (2012)
- Schäfer, W.: *Ecology and Paleocology of Marine Environments*. The University of Chicago Press, Chicago (1972)
- Silva, P.N., Gonçalves, E.C., Rios, E.H., Muhammad, A., Moss, A., Pritchard, T., Glassborow, B., Plastino, A., Azeredo, R.B.V.: Automatic classification of carbonate rocks permeability from ^1H NMR relaxation data. *Expert Syst. Appl.* (2015). <https://doi.org/10.1016/j.eswa.2015.01.034>
- Souza, A.A., Carneiro, G., Zielinski, L., Polinski, R., Schwartz, L., Hurlimann, M.D., Boyd, A., Rios, E.H., Trevizan, W.A., Santos, B.C.C., Machado, V.F., Azeredo, R.B.V.: Permeability prediction improvement using 2D Diffusion-T2 Maps. SPWLA. In: 54th Annual Logging Symposium. (2013)
- Souza Lima, W., Andrade, E.J., Bengtson, P., Galm, P.C.: The Sergipe-Alagoas Basin: geological evolution, stratigraphy and fossil content. *Fundação Paleontológica Phoenix* **65**(1), 31 (2002)
- Sun, H., Vega, S, Tao, G.: Estimation of petrophysical parameters of heterogeneous carbonate rock sample with multi-scale CT imagens. In: International Petroleum Exhibition & Conference, Abu Dhabi. (2016). <https://doi.org/10.2118/183114-ms>
- Tavares, A.C., Borghi, L., Corbett, P., Nobre-Lopes, J., Câmara, R.: Facies and depositional environments for the coquinas of the Morro do Chaves Formation, Sergipe-Alagoas Basin, defined by taphonomic and compositional criteria. *Braz J Geol* (2015). <https://doi.org/10.1590/2317-488920150030211>
- Teixeira, B. F. L.: Coquinas da formação Morro do Chaves (Cretáceo inferior), seção Rifte da Bacia de Sergipe-Alagoas. (2012). <http://hdl.handle.net/11422/5357>
- Teles, A.P., Machado, A.C., Pepin, A., Bize-Forest, N., Lopes, R.T., Lima, I.: Analysis of subterranean Pre-salt carbonate reservoir by X-ray computed microtomography. *J Pet Sci Eng* (2016). <https://doi.org/10.1016/j.petrol.2016.03.008>
- Vasilyev, L., Raouf, A., Nordbotten, J.M.: Effect of mean network coordination number on dispersivity characteristics. *Transp. Porous Media* (2012). <https://doi.org/10.1007/s11242-012-0054-5>
- Washburn, E.W.: The dynamics of capillary flow. *Phys. Rev.* (1921). <https://doi.org/10.1103/PhysRev.17.273>
- Wong, P.-Z.: *Methods in the Physics of Porous Media*. Academic Press, San Diego (1999)
- Zhang, X., Hebing, A.: Pore characterization of reservoir rocks by integrating scal and petrography. In: SCA (2014)
- Zhou, Y., Zhu, D., Hill, D.: A new petrophysical correlation for the permeability of carbonate rocks. In: SPWLA 60th Annual Logging Symposium, The Woodlands (2019)

Publisher's Note Springer Nature remains neutral with regard to jurisdictional claims in published maps and institutional affiliations.